THE AMERICAN SOCIETY OF MECHANICAL ENGINEERS
345 E. 47th St., New York, N.Y. 10017



94-GT-197

# PREDICTION OF TURBULENT FLOW AND HEAT TRANSFER IN A ROTATING SQUARE DUCT WITH A 180 DEG. BEND

**Prabhu S. Sathyamurthy and Kailash C. Karki**
Innovative Research, Incorporated
Minneapolis, Minnesota

**Suhas V. Patankar**
University of Minnesota
Minneapolis, Minnesota



## Abstract

This paper reports the results of a numerical study on the fluid flow and heat transfer in a rotating square duct with 180 deg. bend. The computations are based the standard k-ε turbulence model with wall functions. At a fixed Reynolds number, results have been obtained over a range of Rotation numbers and coolant-to-wall temperature ratios. These results reflect the complex interaction of Coriolis forces, buoyancy forces, and curvature effects. For the outward leg, rotation causes the heat transfer enhancement on the trailing surface and degradation on the leading surface. However, in the inward leg, there is heat transfer degradation on the trailing surface and enhancement on the leading edge. The buoyancy forces cause further degradation in the heat transfer on the leading surface and enhancement on the trailing surface of the outward leg.

## Nomenclature

| | |
|---|---|
| $C_1$, $C_2$, $C_\mu$ | constants in the k-ε turbulence model |
| D | hydraulic diameter |
| h | heat transfer coefficient |
| k | turbulent kinetic energy, thermal conductivity |
| Nu | Nusselt Number = hD/k |
| p | pressure |
| R | radius |
| Re | inlet Reynolds number = $\rho V_{in} D/\mu$ |
| Ro | Rotation number = $\Omega D/V_{in}$ |
| T | temperature |
| $T_{in}$ | coolant inlet temperature |
| $T_w$ | wall temperature |
| U, V, W | velocity components in x, y, z directions |
| $V_{in}$ | mean velocity at the inlet |
| x, y, z | Cartesian coordinates |
| $\Delta\rho/\rho$ | density ratio = $1 - T_{in}/T_w$ |
| e | dissipation rate of turbulence energy |
| $\mu$ | viscosity |
| $\rho$ | coolant density |
| $\sigma_k$, $\sigma_\varepsilon$ | constants of the k-ε model |
| $\sigma_T$ | turbulent Prandtl number |
| $\Omega$ | rotational speed |

## Introduction

Advanced gas turbine airfoils are subjected to high heat loads and internal convection cooling is generally required to maintain acceptable airfoil metal temperatures and to obtain an acceptable blade life. In internal convection cooling, the coolant air from the compressor is introduced through the hub section into the blade interior and discharged from the trailing edge of the blade. The coolant path is a serpentine passage that comprises of several channels aligned with the airfoil streamwise direction, with two adjacent channels connected by a 180 deg. bend. A schematic of a typical internally-cooled blade is shown in Fig. 1. An accurate knowledge of the local heat transfer in cooling passages is crucial for the prediction of blade metal temperatures and, hence, the blade life.

As a result of the flow features associated with rotation, large coolant-to-wall temperature differences, and sharp turns, the heat transfer characteristics of coolant passages are significantly different from those of stationary ducts. For radial outflow in a rectangular duct, the Coriolis force induced by rotation leads to a cross-stream pattern comprising of multiple vortices, which transport fluid from the core toward the trailing edge of the duct. The centrifugal-buoyancy forces, arising due to large coolant-to-wall temperature differences, modify the axial velocity distribution. The presence of sharp turns also leads to a multicellular cross-stream flow pattern, in which the centrifugal forces convect fluid from the core toward the outer surface. In a coolant passage, there is a complex interaction between these individual processes. A better understanding of the Coriolis, centrifugal buoyancy, and curvature effects and the capability to predict them is necessary to design cooling configurations for high performance systems where acceptable blade metal temperatures and high efficiencies must be achieved by utilizing small coolant flow rate.

A large number of studies, both experimental and computational, are available on the effects of rotation and buoyancy on flow in radially rotating passages. Here we restrict our discussion to the recent studies on turbulent heat transfer in passages with smooth walls; details of other studies can be found in the references cited here. Wagner et al. (1991a, b) have provided detailed heat transfer measurements in a serpentine passage consisting of four legs (two up-flow and two down-flow) and three

Presented at the International Gas Turbine and Aeroengine Congress and Exposition
The Hague, Netherlands — June 13–16, 1994

connecting 180 deg. bends. The duct walls in these experiments were maintained isothermal. The first set of results (Wagner, 1991a) were for the first up-flow leg of the passage and indicate that rotation causes an increase in heat transfer over the trailing face. On the leading edge, however, there was a decrease in heat transfer near the inlet, followed by an increase at downstream locations. The second set of results (Wagner, 1991b) were concerned with the first, second, and third radial passages of the serpentine passage. The flow in the first and third passages was radially outward and that in the connecting passage was radially inward. The results indicated that the heat transfer rates were significantly affected by the flow direction.

Soong et al. (1991) have presented heat transfer results for radially rotating isothermal rectangular ducts of various aspect ratios. Results have been presented for Reynolds numbers in the range 700 (laminar flows) to 20,000 (turbulent flows) and show that the effect of Coriolis forces is most significant for ducts with aspect ratios near unity.

Yang et al. (1992) have performed heat transfer experiments in a four-pass serpentine channel of square cross section at low rotational speeds. The results show significant heat transfer enhancement near the sharp turns due to strong secondary flow. These investigators also found that, for the rotational speeds considered, although rotation significantly affects local heat transfer coefficients, it has little effect on the circumferentially averaged heat transfer coefficients.

Chyu (1991) has used the naphthalene mass transfer technique to study heat transfer distributions for flow passing through two-pass and three-pass stationary cooling passages with 180 deg. turns. The results indicate that the two-pass (one-turn) passage produces approximately 45 to 65% higher heat transfer compared to the corresponding straight channel. Further, the results for the three-pass passage indicate that the heat transfer characteristics around the second turn are nearly identical to those around the first turn, implying the attainment of thermally developed conditions at the first turn.

Guidez (1989) has presented an experimental and theoretical study of convective heat transfer in a radially rotating duct of rectangular cross section. The results indicate heat transfer augmentation on the trailing surface and slight deterioration on the leading surface. The numerical results have been obtained using a mixing length model of turbulence and are in qualitative agreement with the experimental data.

In addition to the experimental studies mentioned above, several attempts have been made to numerically predict the flow and heat transfer in radially rotating ducts and ducts with 180 deg. bends. Icovides and Launder (1987, 1990) have reported computations for fully turbulent flow through radially rotating rectangular ducts. The results show a complex secondary flow pattern comprising of counterrotating eddies. Low rotational speeds cause the formation of a pair of symmetric streamwise vortices. At higher rotational speeds, a more complex four-vortex structure develops. Choi et al. (1989) have presented computations for turbulent flow through a stationary 180 deg. bend with a square cross section. In this work, results have been presented using both the eddy viscosity (k-ε) turbulence model and the algebraic stress model. The use of the algebraic stress model led to results that were in good agreement with the experimental data.

Prakash and Zerkle (1992) have presented a computational study of flow and heat transfer in a radially rotating square duct. The standard k-ε model has been used to simulate the effects of turbulence. The computed results are in fair agreement with the experimental data of Wagner et al. (1991a) and indicate that the k-ε model can be used effectively to study the influence of rotation and buoyancy on flow and heat transfer in coolant passages.

In this paper, we present a computational analysis of turbulent flow and heat transfer in a rotating square duct (side length = 0.0127 m) with a 180 deg. bend. This configuration, shown in Fig. 2, simulates the first two passes of a serpentine passage. The flow in the first pass is directed radially outward and that in the second pass is radially inward. The length of the first pass is 14D, the radius of curvature of the bend is 0.5D, and the length of the second pass is also 14D. The radius of the root is 41.9D. The walls of the passage are taken as isothermal. This problem is governed by four parameters: inlet Reynolds number, Rotation number (or the inverse Rossby number), coolant-to-wall temperature ratio, and the radius-to-passage hydraulic diameter ratio. In this study, the inlet Reynolds number and the radius-to-passage hydraulic diameter ratio were fixed at 25,000 and 41.9, respectively; the Rotation number was varied from 0 (stationary passage) to 0.2; and the coolant-to-wall temperature ratio was varied from 0.05 to 0.2. These calculations are made at a system pressure of 1MPa (10 atmospheres). The present computations are based on the k-ε model with the wall-function approach.

During the preparation of this manuscript, we also became aware of the work of Bo and Launder (1992), who have also analyzed flow and heat transfer in a radially rotating U-bend. The results of Bo and Launder (1992) are based on a two-layer turbulence model, in which the high-Reynolds number k–ε model is interfaced with a one-equation near-wall turbulence model. The predicted results are in broad qualitative agreement with the experiments. In contrast to the approach of Bo and Launder, the present computations are based on the k-ε model with wall functions. Since the k-ε model is very widely used and represents a good compromise between accuracy, computational effort, robustness, and general applicability, it is highly desirable to document its performance for rotating serpentine passages. One of the aims of the present study is to provide this information.

## Mathematical Formulation

**Governing Equations.** The coordinate system shown in Fig. 2 rotates with the duct. In this coordinate system, the flow is steady, but the momentum equations include the centrifugal and Coriolis force terms. Using the Cartesian tensor notation, the time-averaged governing equations can be written as:

$$\frac{\partial}{\partial x_i}(\rho U_i) = 0 \tag{1}$$

$$\frac{\partial}{\partial x_j}(\rho U_i U_j) = -\frac{\partial P}{\partial x_i} - \frac{\partial}{\partial x_j}\left[\mu\left(\frac{\partial U_i}{\partial x_j} + \frac{\partial U_j}{\partial x_i}\right) - \rho\overline{u_i u_j}\right] + S_i \tag{2}$$

$$\frac{\partial}{\partial x_i}(\rho U_i T) = -\frac{\partial}{\partial x_i}\left(\frac{\mu}{\sigma_L}\frac{\partial T}{\partial x_i} - \rho\overline{u_i t}\right) \tag{3}$$

where the upper case letters represent time-mean quantities and the lower case letters the fluctuating components. The source terms $S_i$ in the momentum equations include the centrifugal and Coriolis forces. These terms appear in the momentum equations along the x and y directions (see Fig. 2) and are given by the following expressions:

x-component $\quad 2\rho\Omega v + \rho\Omega^2 x$ (4a)

y-component $\quad -2\rho\Omega u + \rho\Omega^2 y$ (4b)

The quantities $\rho\overline{u_i u_j}$ and $\rho\overline{u_i t}$ in Eqs. (2) and (3) represent the turbulent Reynolds stresses and the turbulent heat flux, respectively. The Reynolds stresses are approximated by the high Reynolds number version of the two equation (k-ε) model (Launder and Spalding, 1974). The Reynolds stress is related to the mean rate of strain via a turbulent viscosity

$$-\rho\overline{u_i u_j} = \mu_t\left(\frac{\partial U_i}{\partial x_j} + \frac{\partial U_j}{\partial x_i}\right) - \frac{2}{3}\delta_{ij}\rho k \tag{5}$$

In this expression the turbulent viscosity is calculated from

$$\mu_t = C_\mu \rho \frac{k^2}{\varepsilon} \tag{6}$$

where k and ε are the turbulence kinetic energy and dissipation rate of turbulence energy, respectively, the values of which are obtained from the solution of the modeled transport equations:

$$\frac{\partial}{\partial x_j}(\rho U_j k) = \frac{\partial}{\partial x_j}\left(\frac{\mu_t}{\sigma_k}\frac{\partial k}{\partial x_j}\right) - \rho\overline{u_i u_j}\frac{\partial U_i}{\partial x_j} - \rho\varepsilon \quad (7)$$

$$\frac{\partial}{\partial x_j}(\rho U_j \varepsilon) = \frac{\partial}{\partial x_j}\left(\frac{\mu_t}{\sigma_\varepsilon}\frac{\partial \varepsilon}{\partial x_j}\right) - C_1\rho\overline{u_i u_j}\frac{\partial U_i}{\partial x_j} - C_2\rho\frac{\varepsilon^2}{k} \quad (8)$$

The model constants are assigned the following standard values:

$$C_\mu = 0.09, \quad C_1 = 1.44, \quad C_2 = 1.92, \quad \sigma_k = 1.0, \quad \sigma_\varepsilon = 1.3 \quad (9)$$

The turbulent heat flux $\rho\overline{u_i t}$ is related the gradient of the mean temperature as

$$-\rho\overline{u_i t} = \frac{\mu_t}{\sigma_T}\frac{\partial T}{\partial x_i} \quad (10)$$

where $\sigma_T$ is the turbulent Prandtl number, which is assigned a value of 0.86.

In the present analysis the molecular viscosity and specific heat of the fluid are assumed uniform. The molecular Prandtl number is taken as 0.72. The fluid density ρ is calculated using the ideal gas law:

$$\rho = \frac{p}{RT} \quad (11)$$

For a given geometry, the flow and heat transfer in the rotating passage is governed by four parameters: the inlet Reynolds number Re, the rotation number Ro, the coolant-to-wall temperature difference $\Delta\rho/\rho$ , and the radius-to-passage hydraulic diameter ratio R/D.

**Boundary Conditions.** At the inlet to the duct, the streamwise velocity, kinetic energy, dissipation, and temperature profiles are assumed to be uniform and the cross-stream velocity components are assumed to be zero. The inlet values of the kinetic energy and the rate of dissipation are calculated as

$$k_{in} = 0.04\ V_{in}^2 \quad (12a)$$

$$\varepsilon_{in} = k_{in}^{1.5}/(0.3D) \quad (12b)$$

where $V_{in}$ is the inlet velocity and D is the hydraulic diameter.

The cells adjacent to the walls were treated by the wall functions (Launder and Spalding, 1974). Such a practice eliminates the need for a very fine grid near the walls where the gradients are very steep.

At the outlet section, a zero gradient was used as the boundary condition for all the variables. This condition corresponds to a convection-dominated situation at the outlet.

**Solution Procedure.** The governing equations were solved in a body-conforming coordinate system using the three-dimensional variant of the calculation procedure described by Karki and Patankar (1988). The discretization of the equations is performed in a generalized coordinate system using the finite-volume formulation. A staggered grid arrangement is used in which the scalar quantities are stored at the center of a control volume and the velocity components are displaced along the coordinate directions to lie at the midpoints of the control-volume faces. The momentum equations are written in terms of the physical covariant (grid-oriented) velocity components. The standard derivations of the momentum equations in curvilinear coordinates lead to a large number of additional terms that result from nonorthogonality and curvature of the coordinates. This complication is totally eliminated in the method by Karki and Patankar (1988) by using a locally fixed coordinate system, in which the discretization equation for a particular velocity component is derived in terms of the velocity components, at the neighboring grid points, that are parallel to the velocity component being considered. This formulation results in a compact representation of the curvature source terms that arise due to the spatial variation of the base vectors associated with the covariant velocity components. The power-law differencing scheme (Patankar, 1980) was used to discretize the combined convection-diffusion terms in the transport equations. The coupling between the continuity and momentum equations was handled using the SIMPLER algorithm (Patankar, 1980). The linearized algebraic equations were solved using a modified form of the Stone's algorithm (Stone, 1968), supplemented by a block-correction procedure (Patankar, 1981).

**Computational Details.** The computations were made on an algebraically-generated grid comprising of 95 control volumes in the streamwise direction and 20 control volumes each in the two cross-stream directions. To resolve the thin boundary layers near the inlet, a finer grid spacing was used in that region. The near-wall grid spacings were adjusted to ensure that the $y^+$ values were in the range 20 to 100 so that the wall-function treatment was applicable. The grid arrangement is shown in Fig. 2. The adequacy of the final grid was established by computing several flows in rotating and stationary straight ducts.

The iterative solution of the coupled equations was terminated when the sum of the absolute values of the residuals over all the grid points, normalized by suitable reference quantities, for each equation fell below 0.1%. At this stage of convergence, the sum of the absolute values of the residuals in continuity equation was typically less than $10^{-4}$% of the incoming mass flow rate.

## Results and Discussion

In this section, we present the results for velocity and temperature fields and side-averaged Nusselt numbers for the rotating square duct with a 180° bend, shown in the Fig. 2. First, comparisons with available experimental data are presented, followed by a detailed parametric study of the effects of rotation and centrifugal-buoyancy on the flow structure and heat transfer.

**Stationary Straight Duct.** This is a baseline case that illustrates the applicability of the high Reynolds number k-ε model for the flow parameters employed in this study. A systematic grid refinement study was performed to establish the adequacy of the grid used in the study. For all the Reynolds numbers considered, the Nusselt numbers along the length of the duct were found to be in good agreement with other experimental and numerical results; the fully developed values of the Nusselt numbers were in very good agreement with those obtained from standard correlations.

**Rotating Straight Duct.** This configuration has been extensively investigated both experimentally (e.g., Wagner et al., 1991a) and numerically (Prakash and Zerkle, 1991). Here we provide a comparison of the predicted heat transfer results with the experimental data of Wagner et al. (1991a) to establish the adequacy of the high Reynolds number k-ε model for the range of rotation numbers and coolant-to-wall temperature differences considered in this study. The numerical results of Prakash and Zerkle (1990) indicate that the use of the high Re k-ε model is inappropriate for large rotational speeds (Ro > 0.25) due to the tendency of the flow to laminarize near the leading (suction) surface of the duct. Thus, a low Reynolds number version of the k-ε model is required to adequately model this region of the flow. They also concluded that for the high rotation and large buoyancy cases, the buoyancy terms in the turbulence model need to be included. The turbulence model employed in the present study also does not include the buoyancy terms. Thus, this study also evaluates the performance of the standard k-ε model with no buoyancy terms for the range of rotational speeds (Ro < 0.2) and buoyancy levels ($\Delta\rho/\rho < 0.2$) .

The straight rotating duct configuration presents a symmetric

situation which is exploited here for the reasons of computational economy. Therefore only half the domain length in the z direction (Fig. 2) is included in the computational domain. The parameters used in this case are Re = 25,000, Ro = 0.2, and $\Delta\rho/\rho$ = 0.1. The flow and temperature fields reflect the interaction of the Coriolis and centrifugal buoyancy forces. The velocity and temperature fields compare well with those presented by Prakash and Zerkle (1990). The Coriolis forces set up cross-stream flow pattern (Fig. 3) that distorts the axial velocity profile and pushes the cold core flow towards the trailing surface as seen in Fig. 4. The centrifugal buoyancy further distorts the axial velocity distribution leading to highly nonuniform velocity and, consequently, temperature fields. This leads to an increased heat transfer on the trailing (pressure) surface while the heat transfer rate reduces, in comparison to the stationary duct, on the leading (suction) surface. The predicted side-averaged Nusselt numbers are shown in Fig. 5 and are in qualitative agreement with the data of Wagner et al. (1991a) for the case corresponding to Re = 25,000, Ro = 0.24 and $\Delta\rho/\rho$ = 0.13. The Nusselt numbers in this and subsequent figures are normalized using the standard text book correlation for the fully-developed Nusselt number in a straight duct

$$Nu_o = 0.0176\ Re^{0.8} \tag{13}$$

where the Prandtl number of the fluid is taken as 0.72 for air.

The level of agreement between the current predictions and the experimental data is similar to that obtained by Prakash and Zerkle (1991). Any further improvement in the predictions will require the use of a low Reynolds number version of the turbulence model or the use of second-moment closures (Bo and Launder, 1992).

**Stationary Duct With a 180° Bend.** The purpose of including this case in the present study, along with it being a limiting case of zero rotational speed, is that it provides a convenient means of explaining the complex flow structure observed in rotating U-duct. This flow has also been investigated by Bo and Launder (1992) using a two-layer turbulence model.

For this flow, centrifugal forces in the bend produce a two-cell circulation pattern with the outer side wall as the pressure side and inner side wall as the suction side. Figure 6a shows the secondary flow pattern in the stationary duct with the pre-bend leg showing no secondary flow and the post-bend showing the two-cell structure. Figure 6b show the isotherm pattern in the duct. The pre-bend section shows the core cold flow confined to the center of the duct. In the post-bend section, the secondary currents push the cold flow towards the outer side wall. Consequently, the heat transfer rates are higher on the outer side wall and lower on the inner side wall in the bend and post-bend sections of the duct.

**Rotating Duct With a 180° Bend.** This problems brings together the effects of centrifugal-buoyancy and Coriolis forces in the straight sections of the duct, the centrifugal forces due to the bend, and the effect of buoyancy on this force. Figure 7 shows the cross-stream velocity pattern and the isotherm distributions on selected planes (y = 1 cm, 5 cm, 10 cm, and 14 cm) in the radially outward and inward sections of the duct. The flow parameters for this case are Re = 25,000, Ro = 0.1, and $\Delta\rho/\rho$ = 0.2. The curvature of the bend is kept constant throughout this study.

The flow pattern in outward leg, which reflects the actions of Coriolis and centrifugal-buoyancy forces, is same as that in the straight duct. The elliptic effects due to the presence of the bend are weak and are confined to a small region close to the bend. The core cold (heavier) fluid is pushed towards the pressure surface as seen in Fig. 7b. The post-bend flow shows an intense (in comparison to the secondary flow magnitudes due to Coriolis forces) clockwise circulation which is absent in the stationary duct (Fig. 6a). The rotation-affected radially outward flow, as it enters the bend section of the duct, experiences asymmetric centrifugal forces in the cross section. The heavier cold fluid near the trailing surface experiences larger centrifugal force compared to the lighter fluid near the leading surface of the duct cross section. This causes the fluid near the trailing surface to be thrown towards the outer side wall, resulting in the clockwise circulation seen in the first plane after the bend. Thus the intense secondary flow observed in the post-bend sections of multi-pass coolant channels is due to the interaction of the buoyancy forces and the centrifugal forces in the bend.

In the radially inward flow section of the duct, the flow field is essentially a result of the interaction of the fluid inertia, which carries the clockwise circulation generated in the bend, and the Coriolis force due to rotation. In this section of the duct, the role of the centrifugal buoyancy is to flatten the axial velocity profile, thereby reducing the effect of the Coriolis force. The sense of the Coriolis force is in the opposite direction to that in the radially outward flow. However, for the duct length and flow conditions chosen here, the Coriolis force does not overcome the circulation generated in the bend. The consequence of this complex flow feature in the radially inward section is that the colder core flow now spirals downward, washing each surface.

The effect of this complex flow field is further seen in the side-averaged Nusselt numbers along the duct. (Fig. 8). The Nusselt numbers are normalized using the corresponding values, given by Eq. (13), for the fully-developed flow in stationary square duct. In Fig. 8, the legends NUL, NUT, NUS1, and NUS2 indicate the leading face, trailing face, outer side wall, and inner side wall, respectively. The upward leg shows the leading face heat transfer rates to be lower than the trailing face heat transfer rates. This is the same behavior observed in the rotating straight duct case except very close to the bend. The Nusselt number on the outer side wall is expected to be highest compared to the other walls in the bend section. In the radially inward leg of the flow, the clockwise circulation causes the core colder fluid to migrate towards each wall in a spiral fashion. The Nusselt numbers thus peak in that succession starting from the outer side wall. Towards the exit, the clockwise circulation is weakened by the Coriolis and centrifugal buoyancy forces; no further peaks in Nusselt numbers seen along the duct far downstream of the bend.

**Effect of Rotation.** Figure 9 shows the variation of the side-averaged normalized Nusselt number along the duct in the straight sections of the U-duct for Reynolds number of 25,000 and $\Delta\rho/\rho$ = 0.2. The three rotational speeds considered correspond to Ro of 0., 0.1, and 0.2. In the outward flow leg of the duct (y/D < 14), the leading edge heat transfer is damped and the enhancement at the trailing surface is increased with increasing rotational speed. This effect is due to the secondary flow field set up by the Coriolis forces. Again, in the outward leg the heat transfer on the side surfaces is enhanced with increasing Ro, but the Nusselt numbers remain identical on both the inner and outer sides. This is the consequence of the symmetric flow field in the outward leg of the duct. In the inward leg (y/D >16.3) the increase in rotational speed, improves the heat transfer enhancement on the leading surface whereas on the trailing surfaces heat transfer decreases. The side wall heat transfer in the inward leg of the flow is a consequence of the spiraling flow of the colder core fluid as described in the previous section. The contention of the various forces is too complex to discern a simple overall trend in the behavior of the side wall heat transfer from the available prediction.

**Effect of Buoyancy.** Figure 10 shows the effect of variation in the wall temperature, or the inlet density ratio $\Delta\rho/\rho$, for a fixed Re and Ro on the side-averaged normalized Nusselt numbers. The buoyancy effects are strongest on the leading and the trailing surfaces in the outward leg (y/D < 14). An increased centrifugal-buoyancy force further damps the leading edge heat transfer while improving the enhancement on the trailing surface. In the outward leg, the Coriolis forces set up a secondary flow pattern which causes the core (cold and heavy) fluid to migrate towards the trailing face thereby enhancing the heat transfer on this surface. The slower moving hotter and lighter fluid migrates near the leading surface damping the heat transfer at this surface. The increase in the buoyancy level causes the colder fluid to accelerate thereby leading to sharper gradients of velocity at the trailing face and shallower

gradients at the leading surface. The gradients of the temperatures also become steeper at the trailing face and shallower at the leading face. The effect of buoyancy on the side surfaces in the outward leg and all the surfaces of the inward leg is minimal.

## Concluding Remarks

This paper has presented results of numerical computations of turbulent flow and heat transfer in a rotating square duct with a 180 deg. bend. This geometry is an idealization of the internal cooling passages of the turbine blades. The standard k-ε turbulence model employing the wall function treatment is adopted in this study.

The effects of Coriolis and centrifugal buoyancy forces on the flow in a straight rotating duct are correctly predicted. The Coriolis induced secondary motion is qualitatively in agreement with the experimental and other numerical results. The side-averaged Nusselt numbers also compare favorably with the experimental results. The results indicate that more accurate predictions will involve either a computationally expensive low Reynolds number k-ε model, two-layer model, or second-moment closure model.

The predictions in the stationary duct with a 180 deg. bend showed the centrifugal force generated secondary flow structures in the post-bend section. These secondary flows lead to enhanced heat transfer on the outer side wall. These finding are also qualitatively consistent with available numerical and experimental results.

The rotating duct with a 180 deg. bend shows the effects of Coriolis forces on the flow and heat transfer in the straight outward leg of the duct. The asymmetric maldistribution (density distribution) of the flow as it enters the bend section generates a vigorous clockwise circulation which dominates the flow and heat transfer in the bend as well as in the post-bend section of the duct. The effects of Coriolis force in the inward leg of the duct is much weaker for the flow conditions studied here. The presence of the clockwise rotation has also been reported by Bo and Launder (1992).

Finally, a more elaborate turbulence model is essential for accurate prediction of flow and heat transfer for this complex flow situation. The present results, however, show that the standard k-ε model can correctly predict the qualitative trends in the flow and heat transfer in this configuration with considerable computational economy compared to the more elaborate alternatives.

## Acknowledgments

This research was partially funded by a grant from the Minnesota Supercomputer Institute.

## References

Bo, T. and launder, B.E., 1992, "Turbulent Flow and Heat Transfer in Idealized Blade Cooling Passages," Paper presented at the AGARD/PEP Symposium.

Choi, Y.D., Iacovides, H., and Launder, B.E., 1989, "Numerical Computation of Turbulent Flow in a Square-Sectioned 180 Deg Bend," ASME *Journal of Fluids Engineering*, Vol. 111, pp. 59-68.

Chyu, M.K., 1991, "Regional Heat Transfer in Two-Pass and Three-Pass Passages With 180-deg Sharp Turns," ASME *Journal of Heat Transfer*, Vol. 113, pp. 63-70.

Guidez, J., 1989, "Study of the Convective Heat Transfer in a Rotating Coolant Channel," ASME *Journal of Turbomachinery*, Vol. 111, pp. 43-50.

Iacovides, H., and Launder, B.E., 1987, "Turbulent Momentum and Heat Transport in a square-sectioned Ducts Rotating in Orthogonal Mode," *Numerical Heat Transfer*, Vol. 12, pp. 475-491.

Iacovides, H., and Launder, B.E., 1990, "Parametric and Numerical Study of Fully-Developed Flow and Heat Transfer in Rotating Rectangular Ducts," ASME Paper no. 90-GT-24.

Karki, K.C. and Patankar, S.V., 1988, "Calculation Procedure for Viscous Incompressible Flows in Complex Geometries," *Numerical Heat Transfer*, Vol. 14, pp. 295-308.

Launder, B.E. and Spalding, D.B., 1974, "Numerical Computation of Turbulent Flows," *Computer Methods in Applied Mechanics and Engineering*, Vol. 3, pp. 269-289.

Patankar, S.V., 1980, *Numerical Heat Transfer and Fluid Flow*, Hemisphere.

Patankar, S.V., 1981, "A Calculation Procedure for Two-Dimensional Elliptic Flows," *Numerical Heat Transfer*, Vol. 4, pp. 409-425.

Prakash, C. and Zerkle, R., 1991, "Prediction of Turbulent Flow and Heat Transfer in a Radially Rotating Square Duct," in Heat Transfer in Gas Turbine Engines, ASME HTD-Vol. 188, Elovic, E. and Martin, H.L. (eds.), pp. 1-14.

Soong, C.Y., Lin, S.T., and Hwang, G.J., 1991, "An Experimental Study of Convective Heat Transfer in Radially Rotating Rectangular Ducts," ASME *Journal of Heat Transfer*, Vol. 113, pp. 604-611.

Stone, H. L., 1968, "Iterative Solution of Implicit Approximations of Multidimensional Partial Differential Equations," *SIAM Journal of Numerical Analysis*, Vol. 5, pp. 530-558.

Wagner, J.H., Johnson, B.V., and Hajek, T.J., 1991a, "Heat Transfer in Rotating Passages With Smooth Walls and Radial Outward Flow," ASME *Journal of Turbomachinery*, Vol. 113, pp. 42-51.

Wagner, J.H., Johnson, B.V., and Kopper, F.C., 1991b, "Heat Transfer in Rotating Serpentine Passages With Smooth Walls," ASME *Journal of Turbomachinery*, Vol. 113, pp. 321-330.

Yang, W.J., Zhang, N., and Chiou, J., 1992, "Local Heat Transfer in a Rotating Serpentine Flow Passage," ASME *Journal of Heat Transfer*, Vol. 114, pp. 354-361.

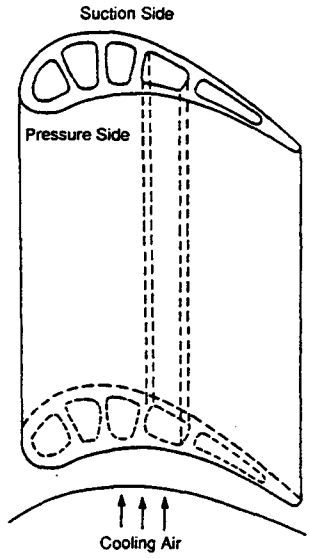


Figure 1 A schematic of a typical internally-cooled turbine blade

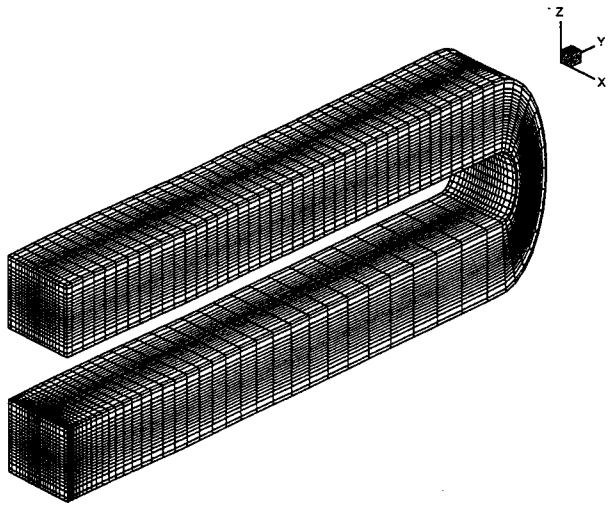


Figure 2 Configuration considered and the computational grid. The axis of rotation is along the z direction and the sense of rotation is counterclockwise.

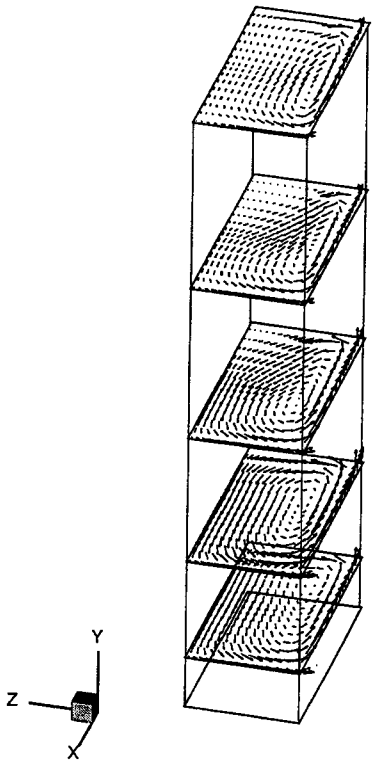


Figure 3 Cross-stream flow patterns for a radially rotating square duct. Only half the square duct is shown with the left boundary as the plane of symmetry.

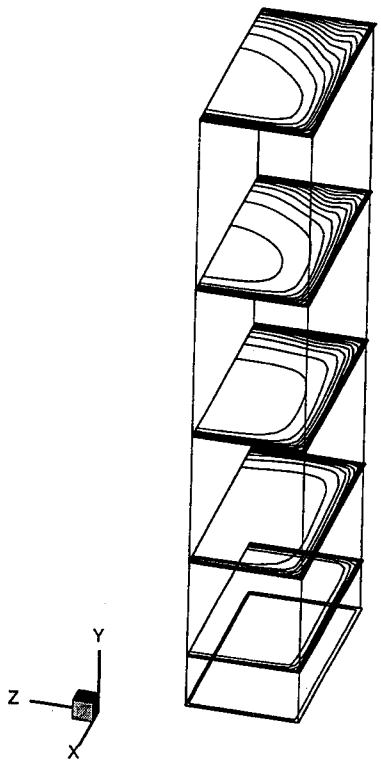


Figure 4 Isotherm patterns for a radially rotating square duct. The section of duct shown is same as in Fig. 3.

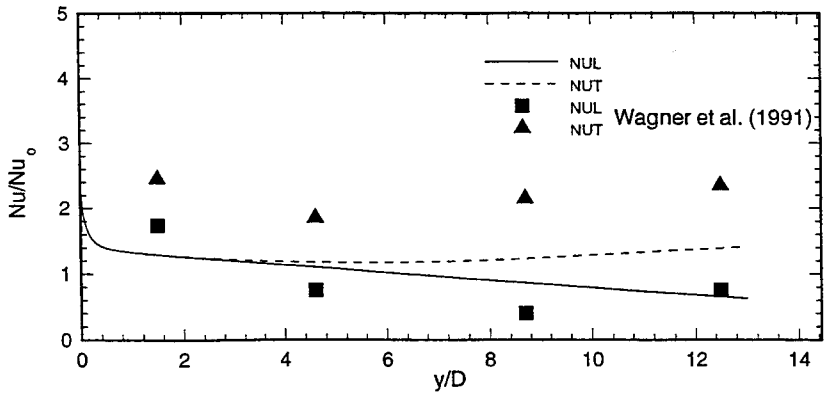


Figure 5 Side-averaged Nusselt numbers for radially rotating square duct. The predictions are compared with the experimental data of Wagner et al. (1991a).

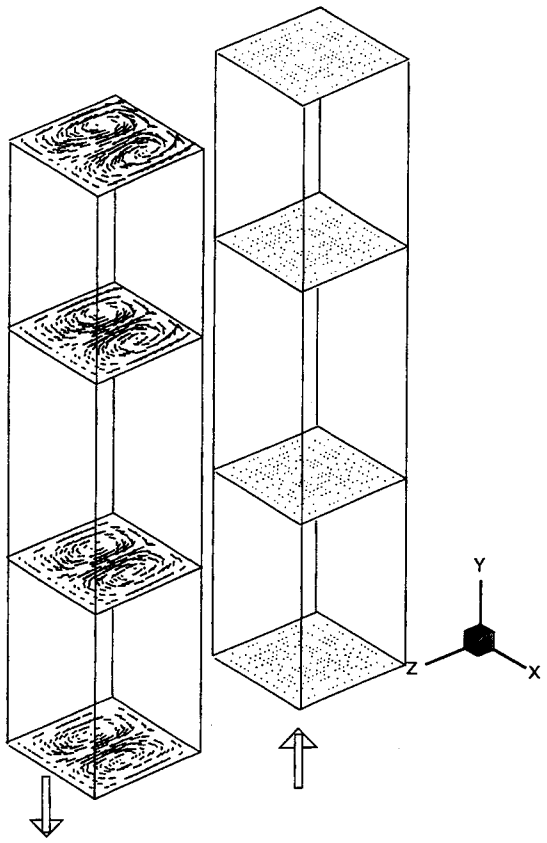


Figure 6a Cross-stream flow patterns for a stationary duct with a 180 deg. bend. The arrows indicate the flow directions. The secondary flow in the inward leg is caused by the centrifugal forces in the bend.

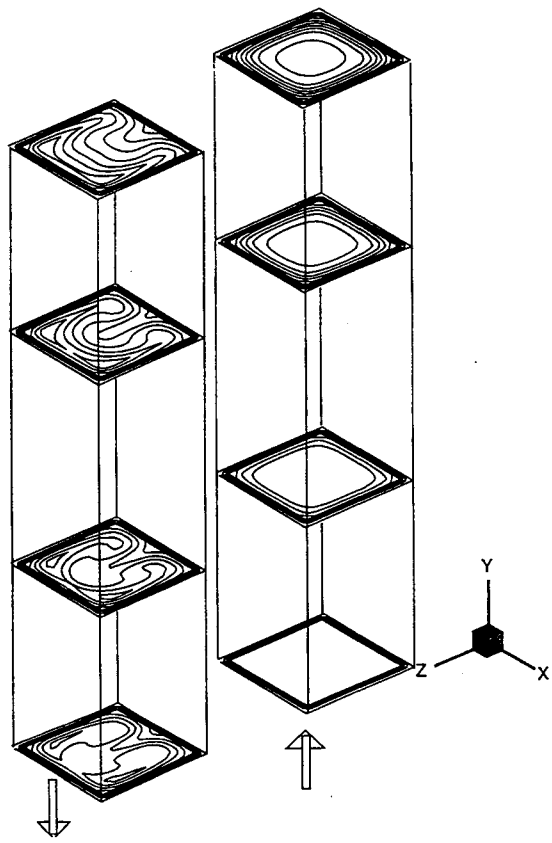


Figure 6b Isotherm patterns for a stationary duct with a 180 deg. bend. The distortion in the isoltherms is due to the secondary flow shown in Fig. 6a.

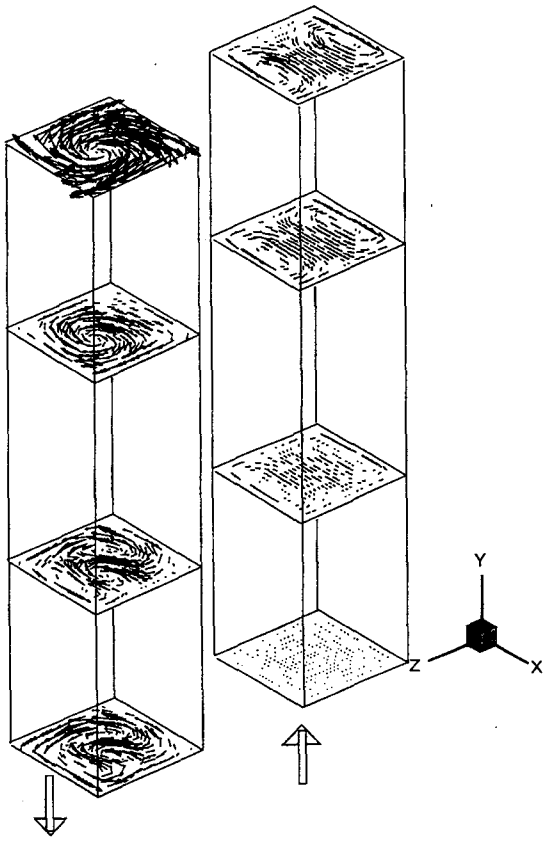


Figure 7a Cross-stream flow patterns for a rotating duct with a 180 deg. bend. The arrows indicate the flow directions. The secondary flow in the outward leg is due to rotation. The flow in the inward leg reflects the interaction of rotation, buoyancy and centrifugal forces in the bend.

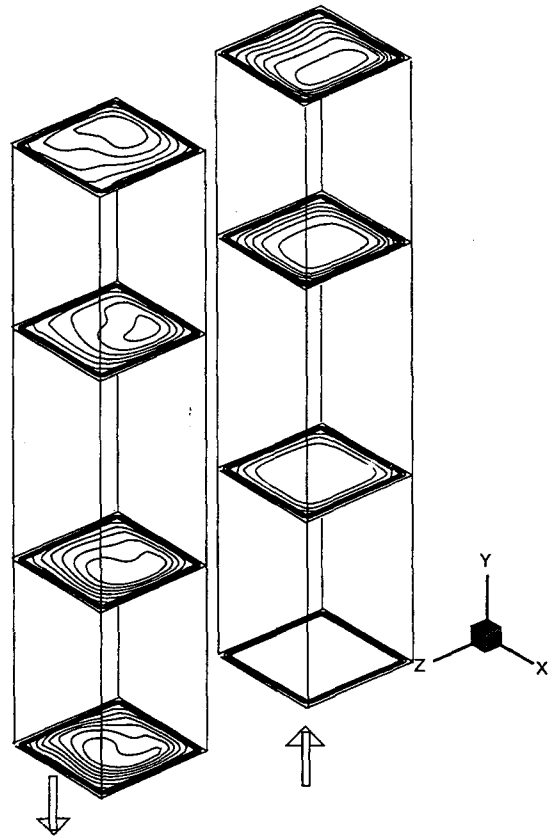


Figure 7b Isotherm patterns for a rotating duct with a 180 deg. bend. The temperature field is a consequence of the secondary flow pattern shown in Fig. 7a.

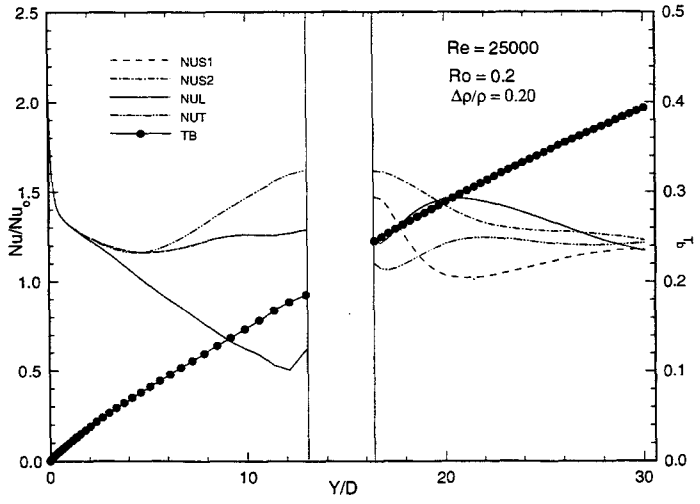


Figure 8 Side-averaged Nusselt numbers for rotating duct with a 180 deg. bend. The legend NUS1, NUS2, NUL, and NUT represent the outer side wall, inner side wall, leading surface and the trailing surface, respectively. TB is the normalized bulk temperature.

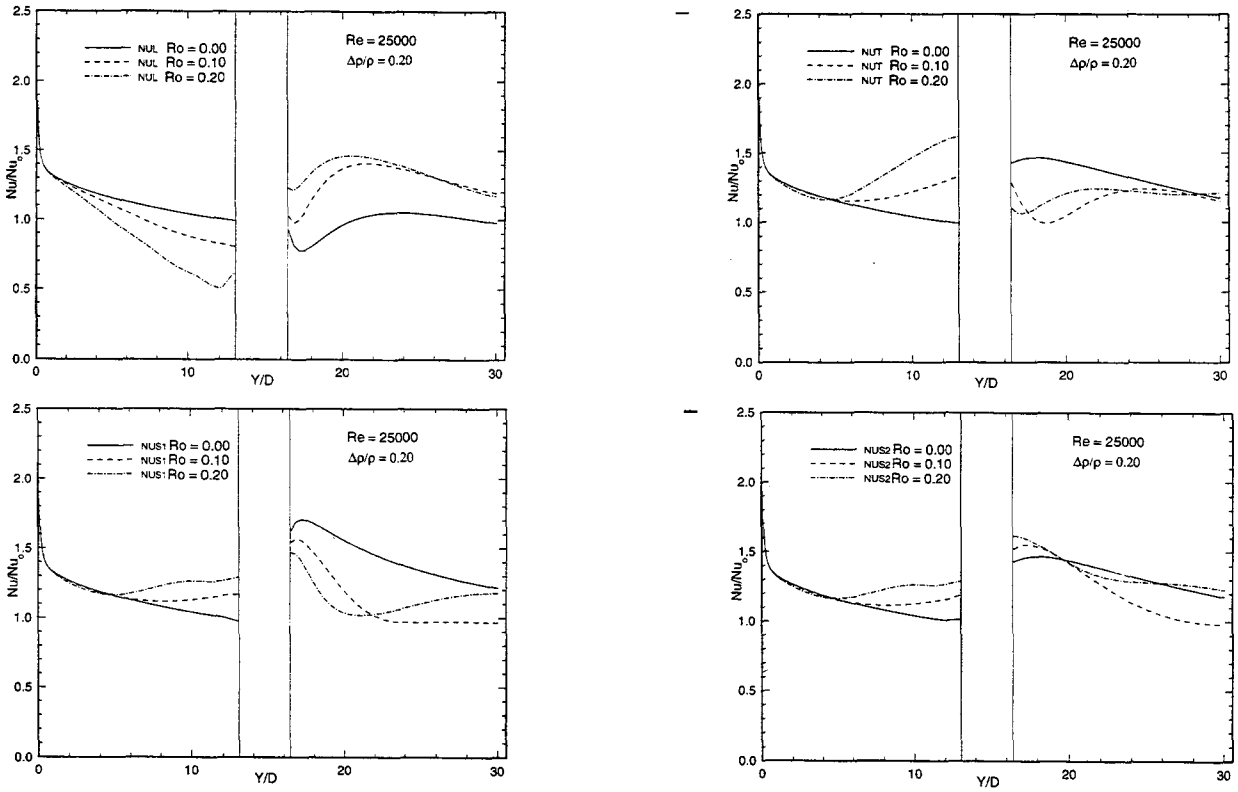


Figure 9 Effect of rotation on side-averaged Nusselt numbers on (a) leading surface, (b) trailing surface, (c) outer side wall, and (d) inner side wall.

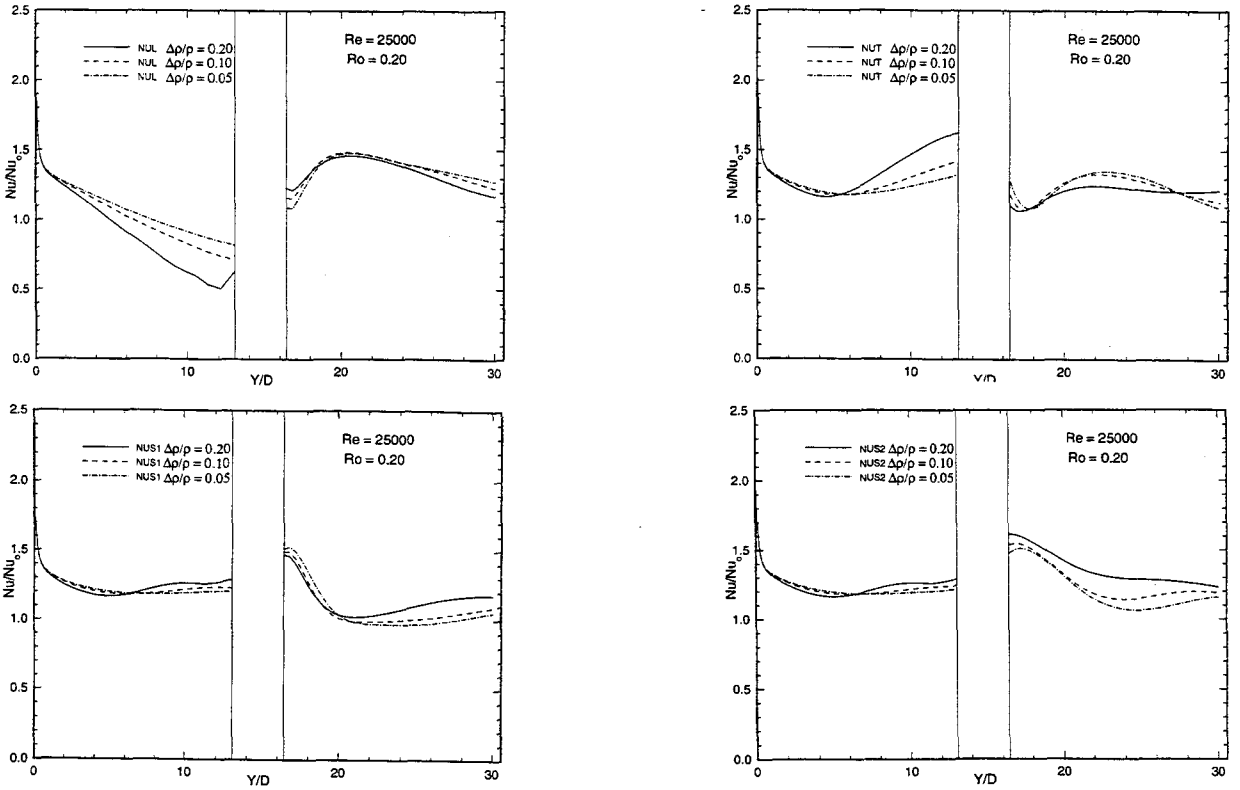


Figure 10 Effect of buoyancy on side-averaged Nusselt numbers on (a) leading surface, (b) trailing surface, (c) outer side wall, and (d) inner side wall.